NON-INVASIVE GROUND-TRUTH VALIDATION IN VEGETATION MONITORING BY AN ULTRA-WIDEBAND GROUND-BASED POLARIMETRIC SAR SYSTEM

Zheng-Shu Zhou[(1)], Tadashi Hamasaki[(1)], Wolfgang-Martin Boerner[(2)] and Motoyuki Sato[(1)]

[(1)] Center for Northeast Asian Studies, Tohoku University, Sendai, 980-8576, Japan
{zszhou, hamasaki, sato}@cneas.tohoku.ac.jp
[(2)] ECE-CSN, University of Illinois at Chicago, Chicago, USA 60607-7018,
boerner@ece.uic.edu

1. INTRODUCTION

The Polarization State of electromagnetic wave scattering is an important feature and a wide range of classification algorithms and inversion techniques have recently been developed based on the transformation of the polarization state by scattering objects [1, 2]. Synthetic Aperture Radar (SAR) can advantageously be exploited in a ground-based radar imaging system, named Ground-Based SAR (GB-SAR). It is a new application of the SAR expansion in the spatial domain. We have extended those earlier approaches [3, 4] and developed an ultra-wideband, ground-based, fully polarimetric SAR system for environmental studies [5]. Polarimetric calibration obviously improved the features of the GB-SAR system. Using the developed SAR system, we carried out measurements on three different kinds of trees in spring, summer and autumn, respectively. 3-D images were reconstructed from the acquired data by a series of signal processing procedures. Analyzing the polarimetric images of each measurement, differences among the different polarizations were found. Further, different polarimetric analysis techniques were employed to interpret the acquired polarimetric data. The results of polarimetric analysis are presented in this report, which show good agreement with ground truth.

2. SYSTEM CALIBRATION AND FIELD EXPERIMENTS

Polarimetric Calibration:

Based on SAR principles and simulation results [6], an ultra-wideband ground-based polarimetric SAR system was developed, as illustrated in Fig. 1. The radar system consisted of a vector network analyzer, a diagonal dual polarized broadband horn antenna, an antenna positioning unit, and a PC-based control unit. The synthetic aperture is realized by scanning the antennas on a horizontal rail and moving along a vertical post. The horizontal and vertical scanning aperture widths determine the horizontal and vertical resolutions. Testing results showed satisfactory polarimetric performance of the developed system [5, 6].

A modified polarimetric Radar Cross Section (RCS) calibration technique using two orientations of the dihedral corner reflectors as calibration targets is introduced [6, 7]. This method is valid for any monostatic or quasi-monostatic radar system. From the theoretical value of two calibrators and measured data, we can recover calibration coefficients. With the use of the calibration coefficients, the auto-calibrated results are presented in Table 1 resulting in observable improvements after calibration, especially in the phase term. Although neglecting effects of noise in the calibration measurement, desired improvements due to calibration have been achieved.

Fig. 1 A developed polarimetric GB-SAR system

ISBN: 4-88552-207-2 C3055©IEICE

Table 1 Auto-calibrated scattering matrices

	Measured scattering matrix	Calibrated scattering matrix
Vertical dihedral	$S_{m1}=\begin{bmatrix}0.9709e^{-j114.8^\circ} & 0.0173e^{-j115.6^\circ}\\ 0.0166e^{-j106.4^\circ} & 1\end{bmatrix}$	$S^c_{m1}=\begin{bmatrix}1.0004e^{-j180.0^\circ} & 0.0186e^{-j109.0^\circ}\\ 0.0182e^{-j116.6^\circ} & 1\end{bmatrix}$
45º dihedral	$S_{m2}=\begin{bmatrix}0.0850e^{-j91.1^\circ} & 1\\ 1.0095e^{j1.4^\circ} & 0.0175e^{-j166.7^\circ}\end{bmatrix}$	$S^c_{m2}=\begin{bmatrix}0.0001e^{j144.5^\circ} & 1\\ 1 & 0\end{bmatrix}$

Field Experiments with the Ultra-wideband Polarimetric GB-SAR System:

Due to the fact that trees are some of the most important factors of the terrestrial vegetation cover, we selected an experimental site with different types of trees used for the non-invasive remote monitoring measurements. The main targets are denoted in Table 2 by T1, T2 and T3, and represent three different kinds of trees. T1 is a Japanese Zelkova, which is a deciduous tree that has no leaf in spring, exuberant broad leaves during early summer up to mid-autumn, after then leaves fall off. T2 is a Japanese cedar, which is an evergreen with needles. It almost does not change from spring to winter. T3 is a kind of shrub of the Azalea genus which is a short bush surrounded by some plants: Japanese honeysuckle. From spring to summer, they have very dense foliage while there are some bare stems and branches after autumn. We have carried out three measurements at the same exact position for the three different trees in late spring (April 19, 2002), in early summer (May 28, 2002) and in late autumn (Nov. 11, 2002), respectively [6]. There were a few fresh leaves during the first measurement in spring. Very significant growth in leaves and branches was observed in the second measurement in summer, while the third measurement was at a time when the leaves had fallen off. HH, VH and VV polarization frequency domain data were acquired which cover the spectral domain of 1 GHz to 5 GHz.

3. NON-INVASIVE GROUND-TRUTH VALIDATION ASSOCIATED DATA INTERPRETATION

Due to different data structure, GB-SAR signal processing is not the same as for airborne SAR data processing. A combined broadband polarimetric GB-SAR data processing procedure associated with band-pass filter, IFFT, time gating, FFT, calibration, matched filter and wave migration algorithms is created [6]. 3-D image reconstruction is obtained via an extended back-projection algorithm [8].

Single Frequency Scattering Matrices:

From migrated data, spatial frequency domain data can be created by Short Time Fourier Transform (STFT) [6]. Three observation points A, B, C from main targets area are selected [6], which correspond to T1, T2 and T3, respectively. At each point, scattering matrix was calculated from their spatial frequency domain data. Scattering matrices of 3 GHz for each measurement and each target are shown as follows in Table 2.

Table 2 Scattering matrices at 3 GHz

	A: Tree 1	B: Tree 2	C: Tree 3
Spring	$\begin{bmatrix}e^{j55.93^\circ} & 0.0199e^{-j117.58^\circ}\\ 0.0199e^{-j117.58^\circ} & 0.5229e^{-j56.58^\circ}\end{bmatrix}$	$\begin{bmatrix}e^{-j146.31^\circ} & 0.6393e^{j34.42^\circ}\\ 0.6393e^{j34.42^\circ} & 0.7574e^{j35.45^\circ}\end{bmatrix}$	$\begin{bmatrix}e^{-j152.92^\circ} & 1.4826e^{-j153.19^\circ}\\ 1.4826e^{-j153.19^\circ} & 1.0974e^{-j150.39^\circ}\end{bmatrix}$
Summer	$\begin{bmatrix}e^{j52.24^\circ} & 0.4803e^{-j123.23^\circ}\\ 0.4803e^{-j123.23^\circ} & 1.5813e^{j54.29^\circ}\end{bmatrix}$	$\begin{bmatrix}e^{j34.67^\circ} & 0.4718e^{j34.36^\circ}\\ 0.4718e^{j34.36^\circ} & 1.3186e^{j34.40^\circ}\end{bmatrix}$	$\begin{bmatrix}e^{j26.49^\circ} & 1.1656e^{-j155.75^\circ}\\ 1.1656e^{-j155.75^\circ} & 1.0230e^{j25.21^\circ}\end{bmatrix}$
Autumn	$\begin{bmatrix}e^{j122.77^\circ} & 0.1329e^{j49.63^\circ}\\ 0.1329e^{j49.63^\circ} & 1.945e^{j54.11^\circ}\end{bmatrix}$	$\begin{bmatrix}e^{j34.86^\circ} & 0.6198e^{j35.47^\circ}\\ 0.6198e^{j35.47^\circ} & 1.2708e^{j38.56^\circ}\end{bmatrix}$	$\begin{bmatrix}e^{-j155.0^\circ} & 0.4570e^{-j152.51^\circ}\\ 0.4570e^{-j152.51^\circ} & 1.0769e^{j25.88^\circ}\end{bmatrix}$

For point A, the HH and VV are dominated due to horizontal scattering features, ground clutter and vertical branches and the trunk of tree T1. Moreover, values of the cross polarization terms in spring and autumn are smaller than the ones for summer. The fact may be that there were many larger leaves in summer to cause stronger VH reflection. We can also find that the co-polarization terms of point B

are dominant but the VH returns are almost alike and stronger than those at point A. It is due to the fact that point B is located at an evergreen tree. The conifer needles and branches cause large VH reflection. For point C, VH terms are stronger than HH and VV terms in spring and in summer due to number leaves and plants. When leaves fall off, the VH term became smaller.

Polarimetric Power Density Images from Covariance Matrix:

A way to visualize the polarimetric information is to transform to the Pauli spin matrix basis, first introduced in this context by Cloude [9]. In the basis of the backscatter case, the Pauli spin target scattering vector can be rewritten as

$$k_s = \frac{1}{\sqrt{2}}\left[S_{hh} + S_{vv} \quad 2S_{vh} \quad S_{hh} - S_{vv}\right]^T \tag{2}$$

Then Pauli covariance matrix is defined as $T^s = \left\langle k_s \cdot k_s^{*T} \right\rangle$ (3)

Note that the diagonal terms of the Pauli covariance matrix are just the magnitudes of the three elements of the Pauli spin target vector squared. Therefore, if we display the three diagonal elements of the Pauli covariance matrix as red for the first term, green for the second term and blue for the third term,

$$T_{11}^s = \left\langle \frac{1}{2}\left|S_{hh} + S_{vv}\right|^2 \right\rangle \quad T_{22}^s = \left\langle 2\left|S_{vh}\right|^2 \right\rangle \quad T_{33}^s = \left\langle \frac{1}{2}\left|S_{hh} - S_{vv}\right|^2 \right\rangle \tag{4}$$

we can interpret red areas as having increased single reflection scattering, blue areas as mostly double reflection scattering, and green areas as diffuse scattering. From these equations, as long as the real part of the cross-correlation between S_{hh} and S_{vv} is positive, which means that the co-polarized phase we can interpret red areas as having increased single reflection scattering, blue areas as mostly double reflection scattering, and green areas as diffuse scattering. From these equations, as long as the real part of the cross-correlation between S_{hh} and S_{vv} is positive, which means that the co-polarized phase difference is less than 90 degrees, the first term will be larger than the third. The image will exhibit a red color. When the real part of the cross-correlation between S_{hh} and S_{vv} is negative, which means the co-polarized phase difference is greater than 90 degrees, the third term will be large than the first and the image will exhibit a blue color.

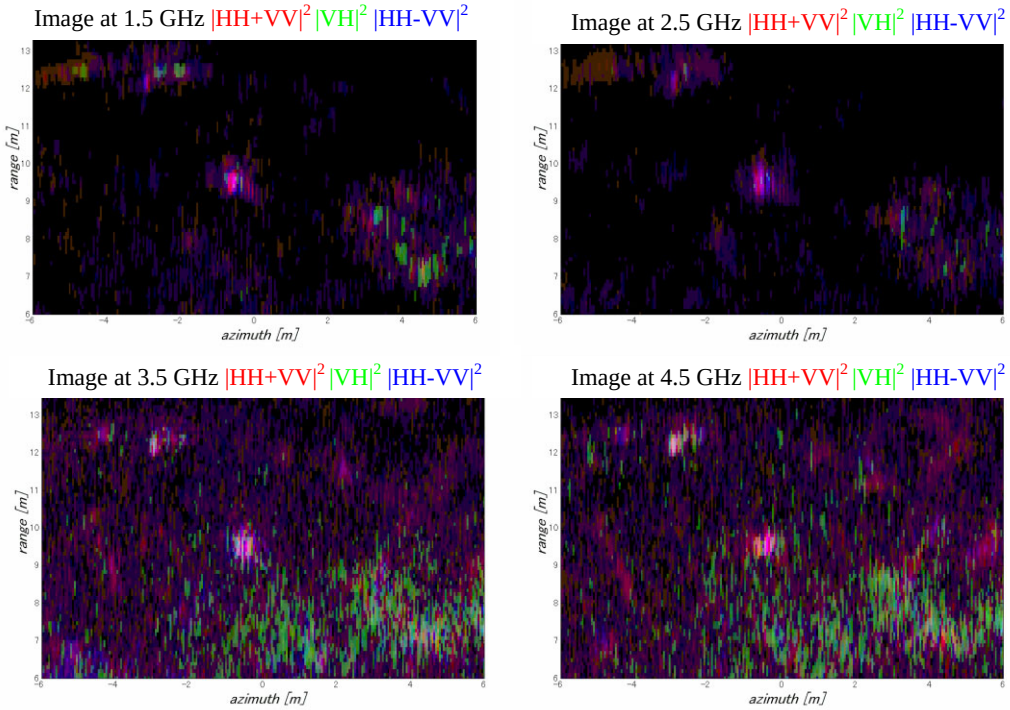

Fig. 2 Polarimetric power density profiles of trees in spring at 2.5m above ground

The polarimetric power density images of 1.5 GHz, 2.5 GHz, 3.5 GHz and 4.5 GHz based on diagonal terms of Pauli covariance matrix for the first measurement in spring are shown in Fig. 2. Here complex spatial-frequency domain data were produced from the migrated data by STFT. For lower frequency images of 1.5 GHz and 1.5 GHz, the blue colors are dominant. It means that the real part of the cross-correlation between S_{hh} and S_{vv} is negative, which means the co-polarized phase difference is greater than 90 degrees and double bounce scattering happened. Hence, blue colors indicate scattering of double reflections more than from the ones of single reflections. The concentrated areas interpret the main trunks of trees. With frequency increased, the green color areas become more dominant and larger in 3.5 GHz and 4.5 GHz images. It means that diffuse scattering terms are dominant. It is caused by diffuse scattering mechanisms of leaves and inclined branches, which become negligible compared to the wavelength at low frequency. Small scatterers have shown strong backscattering features at high frequency. However, the blue colors still remain in the images of high frequencies due to the double bounce scattering from trunks and ground.

4. CONCLUSIONS

Development of an ultra-wideband polarimetric GB-SAR system and its non-invasive application to vegetation monitoring were analyzed. A modified two-way oriented dihedral based polarimetric calibration method was introduced and improvement was verified. Continued data acquisitions were carried out for three different types of trees in three seasons. Novel signal processing methods used were effective for broadband ground-based polarimetric SAR data interpretation. Different analysis tools for viewing and interpreting broadband polarimetric SAR data could indicate scattering mechanisms for vegetation and exhibit slight differences of variation of tree species. At the same time, a ground-based SAR system also can be used as ground truth demonstration and validation tool for airborne SAR and space-borne SAR in a great variety of applications.

ACKNOWLEDGEMENT

A part of this work was supported by the Grant-In-Aid for Scientific Research (S)14102024 of the Japanese Ministry of Education, Culture, Sports, Science and Technology.

REFERENCES

[1] W-M. Boerner, “Recent Advances in Extra-wideband Polarimetry, Interferometry and Polarimetric Interferometry in Synthetic Aperture Remote Sensing, and its Applications,” *IEE Proc. Radar Sonar Navigation, Special Issue of the EUSAR-02,* vol. 150, no. 3, pp. 113-125, June 2003.

[2] E. Pottier, S. R. Cloude and W.-M. Boerner, “Recent Development of Data Processing in Polarimetric and Interferometric SAR; Invited Paper, Radio Science Bulletin,” (ed. R.W. Stone), *Special Issue on URSI-GA-03*; Maastricht; NL, RSB-304, March 2003, pp. 48-59, ISSN 1024-4530.

[3] D. Tarchi, E. Ohlmer and A. Sieber, “Monitoring of Structural Changes by Radar Interferometry,” *Research in Nondestructive Evaluation.* vol. 9, pp. 213-225, 1997

[4] M. Pieraccini, G. Luzi and C. Atzeni, “Terrain Mapping by Ground-Based Interferometric Radar,” *IEEE Trans. Geosci. Remote Sensing*, vol. 39, no. 10, pp. 2176-2181, Oct. 2001

[5] Z.-S. Zhou, and M. Sato, “Ground-Based Polarimetric SAR Systems for Environment Study,” *Proc. IEEE AP-S 2003 Digest*, vol. 1, pp.202-205, Columbus, OH. USA, June 2003.

[6] Z.-S. Zhou, *Application of a Ground-based Polarimetric SAR System for Environmental Study,* Doctoral Dissertation of Tohoku University, Japan, August 2003.

[7] J.-R. J. Gau and W. D. Burnside, “New Polarimetric Calibration Technique Using a Single Calibration Dihedral,” *IEE Proc. Microw. Antennas Propag.*, vol. 142, no. 1, February 1995, pp. 19-25.

[8] M. Soumekh, *Synthetic Aperture Radar Signal Processing*, New York: John Wiley & Sons, 1999, pp. 212-215.

[9] S. R. Cloude, “Uniqueness of Target Decomposition Theorems in Radar Polarimetry,” In *Direct and Inverse Methods in Radar Polarimetry: Part 1,* W.-M. Boerner (Ed.), pp. 267-296, Kluwer Academic Publishers, Dordrecht, 1992.